Developmental Biology 340 (2010) 613–625

Contents lists available at ScienceDirect

Developmental Biology

journal homepage: www.elsevier.com/developmentalbiology

Neural crest cell-specific deletion of *Rac1* results in defective cell–matrix interactions and severe craniofacial and cardiovascular malformations

Penny S. Thomas [a,1], Jieun Kim [a,1], Stephanie Nunez [a], Michael Glogauer [b], Vesa Kaartinen [a,*]

[a] *Biologic and Materials Sciences, University of Michigan School of Dentistry, Ann Arbor, Michigan, USA*
[b] *The Canadian Institutes of Health Research Group in Matrix Dynamics and Dental Research Institute, Faculty of Dentistry, University of Toronto, Toronto, Ontario, Canada*

ARTICLE INFO

Article history:
Received for publication 8 October 2009
Revised 12 February 2010
Accepted 12 February 2010
Available online 23 February 2010

Keywords:
Rac1
Neural crest
Craniofacial
Cardiac
Embryogenesis

ABSTRACT

The small GTP-binding protein Rac1, a member of the Rho family of small GTPases, has been implicated in regulation of many cellular processes including adhesion, migration and cytokinesis. These functions have largely been attributed to its ability to reorganize cytoskeleton. While the function of Rac1 is relatively well known *in vitro*, its role *in vivo* has been poorly understood. It has previously been shown that in neural crest cells (NCCs) *Rac1* is required in a stage-specific manner to acquire responsiveness to mitogenic EGF signals. Here we demonstrate that mouse embryos lacking *Rac1* in neural crest cells (*Rac1*/*Wnt1-Cre*) showed abnormal craniofacial development including regional ectodermal detachment associated with mesenchymal acellularity culminating in cleft face at E12. *Rac1*/*Wnt1-Cre* mutants also displayed inappropriate remodelling of pharyngeal arch arteries and defective outflow tract septation resulting in the formation of a common arterial trunk ('persistent truncus arteriosus' or PTA). The mesenchyme around the aortic sac also developed acellular regions, and the distal aortic sac became grossly dysmorphic, forming a pair of bilateral, highly dilated arterial structures connecting to the dorsal aortas. Smooth muscle cells lacking *Rac1* failed to differentiate appropriately, and subpopulations of post-migratory NCCs demonstrated aberrant cell death and attenuated proliferation. These novel data demonstrate that while *Rac1* is not required for normal NCC migration *in vivo*, it plays a critical cell-autonomous role in post-migratory NCCs during craniofacial and cardiac development by regulating the integrity of the craniofacial and pharyngeal mesenchyme.

Introduction

Craniofacial and cardiac malformations are among the most common birth defects in humans. Their pathogenesis often involves cranial neural crest cells (NCC), a migratory, pluripotent population of cells originating from dorsal neural tube from midbrain to third somite levels (Le Douarin et al., 2004; LeDouarin, 1982). In the mouse, this migration starts as the neural plate folds around the 4–5 somite pairs stage, embryonic day 7.5 (E7.5)(Gilbert, 2006; Nichols, 1986). The most rostral cranial NCCs migrate to the frontal nasal process and the maxillary processes of the first pharyngeal arch, where they form most of the skull, and the mesenchymal structures of the developing maxilla, respectively. Cranial NCCs from the hindbrain level populate the mandibular process of the first pharyngeal arch, and the second and third pharyngeal arches, where they form the mesenchymal derivatives of the mandible, neck and pharyngeal organs (Chai et al., 2000). The most caudal cranial NCCs (from rhombomeric level 5 to somatic level 3) are known as the cardiac neural crest (Creazzo et al., 1998). These cells contribute to the smooth muscle cell layer covering the ascending aorta and derivatives of the third, fourth and sixth aortic arch arteries (PAA3, 4 and 6). A subpopulation of cardiac NCCs forms the aortico-pulmonary (AP) septum, and migrates into the outflow tract (OFT) cushions of the heart, playing an important role in the formation of separate aortic and pulmonary valves and trunks (Jiang et al., 2000).

Crucial to the onset of NCC migration are changes in cell shape and formation and maintenance of subcellular structures such as filopodia and lamellipodia that facilitate cell migration (Ridley et al., 2003). Many aspects of these are dependent on the complex functions of small Rho-related GTPases that act as molecular switches and regulate rapid assembly and destruction of actin filaments (Kaibuchi et al., 1999). The Rho small GTPase protein family consists of Rho, Cdc42 and Rac subfamilies (Ridley, 2006). Each member has been suggested to have its own cell-type-specific functions. For instance, in Swiss 3T3 fibroblasts, RhoA, Cdc42 and Rac1 regulate the formation of actin stress fibers, filopodia and lamellipodia, respectively (Ridley and Hall, 1992; Ridley et al., 1992). The Rac subfamily is composed of three members: Rac1, Rac2 and Rac3 (Haataja et al., 1997). Rac1 is expressed ubiquitously. Rac2 expression is limited to hematopoietic tissues and Rac3 is predominanty expressed in the central nervous system. Other important functions of Rho-related GTPases include regulation of cell proliferation, migration, apoptosis and gene

* Corresponding author.
E-mail address: vesak@umich.edu (V. Kaartinen).
[1] Equal contribution.

0012-1606/$ – see front matter © 2010 Elsevier Inc. All rights reserved.
doi:10.1016/j.ydbio.2010.02.021

expression (Aznar and Lacal, 2001; Fukata and Kaibuchi, 2001; Fukata et al., 2003).

Mouse embryos deficient in *Rac1* fail to form appropriate germ cell layers and die at gastrulation (Sugihara et al., 1998). *Rac1*-deficient neutrophils display defects in inflammatory recruitment, migration to chemotactic stimuli, and chemo-attractant-mediated actin assembly (Glogauer et al., 2003). Similarly, deletion of *Rac1* in endothelial cells causes defects in their migration and in angiogenesis (Tan et al., 2008). It has recently been reported that, rather than being necessary for migration, *Rac1* is required in NCCs in a stage-specific manner to acquire responsiveness to mitogenic EGF signals (Fuchs et al., 2009). Here we extend and complement the findings of this study by examining the effects of *Rac1* deficiency in NCCs on craniofacial and cardiovascular development. Our results show that *Rac1* in cranial NCCs is required for normal face and cardiovascular morphogenesis. Lack of *Rac1* in cranial NCCs *in vivo* leads to localized defects in integrity of adhesion between epithelia and underlying NC-derived mesenchyme, severe mid-face clefting, regional apoptosis of post-migratory pharyngeal NCCs, defective differentiation of muscle cells adjacent to the aortic sac and aortic arch arteries, and abnormal morphogenesis of the cardiac outflow tract and great arteries.

Materials and methods

Mouse breeding, genotyping and generation of embryos for analysis

Wnt1-Cre mice were obtained from the Jackson Laboratories and generation of $Rac1^{FXFX}$ and *R26R* mice has been described earlier (Glogauer et al., 2003; Soriano, 1999). $Rac1^{Fx/Fx}$ or $Rac1^{Fx/Fx}$/*R26R*+/+ female mice were crossed with $Rac1^{Fx/+}$/*Wnt1-Cre* male mice to obtain timed pregnancies. As the dark period was 2 am–2 pm, the presence of vaginal plug was designated as embryonic day 0 (E0). DNA for genotyping was prepared from yolk sac or tail lysate using DirectPCR Lysis Reagents (Viagen Biotech). $Rac1^{fx/fx}$ and *Wnt1-Cre* mice were genotyped by PCR as described in the text of supplemental Fig. 1 and in (Glogauer et al., 2003). To prolong the life of mutant genotype embryos, some females were treated with 200 μg/ml isoproterenol delivered in drinking water (Morikawa and Cserjesi, 2008). Pregnant females were euthanized with CO_2 according to National and Institutional guidelines. Embryos were genotyped using yolk sac DNA.

Histology, immunochemistry, cell death and proliferation assays

Embryos were collected at stages of interest, rinsed in PBS, fixed overnight in 4% buffered paraformaldehyde at 4 °C, washed, dehydrated and embedded in Leica Histowax. 7 μm sections were stained with haematoxylin and eosin using a standard protocol. Smooth muscle α-actin antibody (M 0851, 1:50, DAKO) binding was detected using biotin–streptavidin HRP kit (Zymed) and mounted in Immumount (Thermoscientific), or Alexafluor-594 goat anti-mouse (Invitrogen) and mounted as below. Anti-striated muscle myosin antibody (MF20, 1:500 after heat retrieval, DSHB) binding was detected using Alexafluor goat anti-mouse (Invitrogen) and mounted as below. Apoptotic cells were detected using Dead End Fluorometric TUNEL system (Promega) following manufacturer's instructions. Cell proliferation was assessed using Cell proliferation labelling reagent (RPN201, 200 μl ip injection), and then anti *BrdU* antibody (RPN202, GE Healthcare/Amersham) on tissue sections following antigen retrieval, detected using Alexafluor-488 goat anti-mouse antibodies (Invitrogen) and mounted in Vectashield with propidium iodide or with DAPI nuclear stain (Vector Labs Inc). Anti phospho-histone H3 antibody (after antigen retrieval, 9701, 1:50, Cell Signaling) binding was detected using Alexafluor antibodies and mounted as above. Fluorescent images were viewed on an Olympus BX51 with fluorescence attachments and photographed using an Olympus DP71 camera and DP controller and manager software.

R26R fate determination assay and cell shape analysis

Embryos at stages of interest, cultured cells or tissues were rinsed several times in DPBS, fixed in 4% buffered paraformaldehyde or 0.25% buffered glutaraldehyde for 5–15 min at 4 °C, washed and stained using a standard β-galactosidase staining protocol including X-gal (Soriano, 1999), washed in detergent rinse or PBS and fixed. Whole-mounts and cultures were examined using a Leica MZ95 dissecting microscope and photographed as above). Some embryos were processed for wax embedding and sectioned at 7 μm and mounted in Immu-mount (Thermoscientific), then examined on Olympus BX51 microscope and photographed as described previously. For cell shape studies, 80 cells were selected randomly from four separate high resolution images per outflow tract and analyzed using DP Manager and Excel software. Each analysis was performed with at least three independent samples.

Whole-mount in situ hybridization and immunohistochemistry

Whole-mount immunohistochemistry was performed as described (Hogan et al., 1994) using anti-neurofilament 2H3 (DSHB) and anti-Pecam1 (CD31, 550274, BD-Pharmingen) antibodies. Binding was detected using biotin–streptavidin HRP (Zymed) and SigmaFastTM DAB with Metal Enhancer Tablet Set.

For whole-mount RNA in situ hybridization, embryos were collected on ice, fixed in 4% buffered formaldehyde for 12 h and dehydrated with ethanol. Antisense RNA probes were synthesized with NTP DIG RNA labelling mix (Roche Applied Science) following manufacturer's instructions. Probe templates for *Krox20*, *Cad6*, *EphA4* and *Sox10* were obtained from R. Maxson (Keck School of Medicine, USC (Ishii et al., 2005)) and for *Pitx2* and *Axin2* from S. Bellusci (Childrens Hospital Los Angeles (De Langhe et al., 2008)). *Bmp2*, *Bmp4*, *Msx1* and *Msx2* templates, and ISH protocol, were as previously described (Kaartinen et al., 2004). Each analysis was performed with at least three independent samples.

Transmission electron microscopy

Embryos at E11 were rapidly recovered, washed with DPBS on ice and processed according to protocols used by the Microscope Image Analysis Laboratory (University of Michigan Medical School). Briefly, tissues were fixed in 4% paraformaldehyde (EM grade), 2.5% glutaraldehyde in cacodylate buffer at 4 °C overnight. After several washes to remove the fixative, tissues were further dissected to isolate regions for sectioning. These were refixed as above for several days, post-fixed in osmium tetroxide, *en bloc* stained in uranyl acetate and dehydrated to propylene oxide. They were then infiltrated and embedded in Epon resin. Semi-thin sectioning was performed to identify regions of interest and ultra thin sections collected, post-stained with uranyl acetate and lead citrate and examined on a Philips CM100 transmission electron microscope operated at 60KV. High resolution images were recorded digitally using a Hamamatsu ORCA-HR camera system, operated using AMT software (Advanced Microscopy Techniques, Danvers, MA).

Isolation of neural crest cells from the 1st pharyngeal arch

Maxillary and mandibular processes were dissected from E10 embryos in PBS using microscissors. The isolated tissues were dissociated using trypsin (0.25%), and single cell suspensions plated on fibronectin, laminin or collagen-coated dishes (all from BD Biosciences), cultured at 37 °C, 8% CO_2 for 3–4 days, and stained for β-galactosidase activity as described above (*R26R* fate determination

assay). For immunofluorescence, cultured cells were fixed for 5 min with 4% buffered paraformaldehyde. Antibodies specific for FAK (05-537, Upstate) and β-galactosidase (ab616 abcam), and FITC-phalloidin (77415, Sigma), were detected, visualized and recorded as described previously. In some experiments, cells were serum-starved for 2 h and stimulated with 100 ng/ml each of epidermal growth factor (human recombinant EGF, Sigma) and basic fibroblast growth factor (human bFGF, Sigma) for 1 h. Each analysis was performed with at least three independent samples.

2D Neural tube culture

E9 embryos were collected in HBSS on ice. Isolation of individual neural tubes was achieved by removing the head and tail regions and treating the trunk segment with 0.15% dispase for 10–15 min whilst triturating with a pipette to loosen and displace all remaining non-neural tube cells. They were then washed in HBSS/10%FBS to inhibit further dispase activity. Isolated tubes were placed on collagen-coated tissue culture dishes and incubated in DMEM/F-12 (Invitrogen) containing 10%FBS (Invitrogen), 1× Pen Strep (Sigma) and 1× ITS (Invitrogen) at 37 °C 8% CO_2 for 48 h. They were then washed, fixed and stained for β-galactosidase activity (see *R26R* fate determination assay above). Five independent samples were used for this assay.

Immunoblotting

First pharyngeal arch tissues were harvested, snap-frozen and stored at −80 °C until genotype known. Selected arches (pools of three controls and mutants) were then lysed in 2× Laemmli lysis buffer (Harlow and Lane, 1988). Proteins were resolved on NuPAGE BisTris SDS-PAGE gels (Invitrogen) using the X-Cell *SureLock* Mini-Cell electrophoresis system (Invitrogen) according to the manufacturer's instructions. After electrotransfer to PVDF membrane, the filters were blocked (5% milk in TBST) and probed with specific monoclonal anti Rac1 (ARC03; 1:1000, Cytoskeleton Inc) and anti β-Actin (A1978; 1:2000, Sigma) antibodies, followed by HRP-conjugated anti-mouse antibodies. Immunoblots were visualized using ECL reagents (Immobilon, Amersham) and BioSpectrum AC imaging system (UVP).

Results

We deleted *Rac1* in mouse in neural crest cells (NCC) by crossing females homozygous for the floxed *Rac1* allele ($Rac1^{Flox/Flox}$) with males heterozygous both for the floxed *Rac1* allele and *Wnt1-Cre* transgene ($Rac1^{Flox/+}$/$Wnt1\text{-}Cre^{+/-}$) (Danielian et al., 1998; Glogauer et al., 2003). The resulting $Rac1^{Flox/Flox}$/$Wnt1\text{-}Cre^{+/-}$ mice (herein designated *Rac1*/*Wnt1-Cre*, or 'mutant') had exon 1 of the *Rac1* gene deleted. Rac1 protein was absent in the NC lineage by at least as early as embryonic day 10 (E10)(Suppl. Fig 1). Littermates with the other genetic combinations generated were used as controls. Embryos from crosses to generate *Rac1*/*Wnt1-Cre* mice were recovered at different embryonic stages and genotyped. The mutant genotype (*Rac1*/*Wnt1-Cre*) was not lethal until E12, when occasional live mutants were very edematous, unlike control littermates. Treatment of pregnant mothers with isoproterenol enabled the occasional survival of *Rac1*/*Wnt1-Cre* embryos to E13, suggesting a noradrenergic deficiency might play some role in the early lethality.

Rac1/*Wnt1-Cre mutants develop severe craniofacial defects*

At E10, mutant embryos appeared superficially indistinguishable from controls. This was the case even for the pharyngeal arches, largely populated by migrating NCCs (Figs. 1A–B). However, even at this early stage, localized regions of detachment of the epithelial surface ectoderm from its underlying mesenchyme were detectable on the lateral aspects of the first pharyngeal arches in some mutant embryos (Fig. 1D). At E11, heads of mutants were noticeably wider (Fig. 1H and Suppl. Fig. 2), and the medial nasal processes further apart than in controls (Fig. 1H) where they were in direct contact with one another (Fig. 1G). By this stage, very prominent and blister-like epithelial detachment on the lateral parts of the mandibular arches was consistently present (Fig. 1F). Histological analysis confirmed this, but also that pharyngeal arches otherwise contained plentiful relatively normal-appearing mesenchymal cells. In addition, the vascular beds of the first pharyngeal arch in control and mutants appeared indistinguishable at E10 (Figs. 4F, H).

Epithelial detachment was also obvious in the facial midline at E11 (Figs. 1F and 2D). At E12, all surviving mutant embryos showed severe mid-facial clefting (Fig. 1J), likely the result of failure of left and right medial nasal processes to fuse, along with a more extensive region of epithelial detachment in the midline. The arch blister phenotype, prominent on the mandibular arch at E11, was now consistently seen on the maxillary processes too (Fig. 1J). At E13, in addition to the cleft face, the mid-face blisters were even more extensive and also blood-filled (Fig. 1N and Suppl. Fig. 2D). The mutant heads remained much wider than those of controls, the ventricular lumen in particular being larger. In contrast, the amount of craniofacial mesenchyme was considerably less in mutants than in controls; in particular, the posterior palatal shelves were rudimentary when compared to those of control littermates (Figs. 1O–R).

The *R26R* fate determination assay (Soriano, 1999) confirmed that even by E10 the distribution of NC-derived cells in *Rac1*/*Wnt1-Cre* mutants was detectably different in developing facial processes when viewed *en face* from that of corresponding control littermates (Figs. 2A–B). While differences in gross head width at this early time point were not so evident, the darkly staining accumulated NC-derived cells in controls formed a narrower V-shaped pattern, reflecting more medially located boundaries on each side, while the corresponding cell populations in the mutants were further apart. At E10 there were few if any cells in the midline even in controls (data not shown) but by E11, the lack of cellularity in the midline region associated with epithelial blistering was obvious (Figs. 2C–D). In addition, at a more rostral horizontal level, the NC-derived mesenchymal cells remained predominantly in a more lateral position, while the midline region was consistently hypo- or acellular (Figs. 2E–F).

Molecular mechanisms underlying many aspects of craniofacial morphogenesis have been established, so to examine if Rac1 is upstream of the expression of known key players in NC-derived mesenchyme or adjacent ectodermal structures, whole-mount RNA ISH was performed to examine the distribution of *Bmp2* and *Bmp4* (encoding members of the Tgf-β superfamily), their downstream targets, homeobox genes *Msx1* and *Msx2*, in NC-derived mesenchyme and *Pitx2* and *Fgf8* in the interacting craniofacial ectoderm (Liu et al., 2003, 2005; Meyers et al., 1998) at E10 and E11. We could not detect any noticeable differences in expression of any of these genes between *Rac1*/*Wnt1-Cre* mutants and their control littermates (Suppl. Fig. 3, and data not shown). A recent study demonstrated that Rac1 activation controls the nuclear localization of β-catenin (Wu et al., 2008). However, the β-catenin/TCF target gene *Axin-2* was similarly expressed in both *Rac1* mutants and controls at E11, suggesting that *Rac1* is not required for appropriate Wnt/β-catenin signaling in NCCs (Suppl. Fig. 3).

Depletion of Rac1 in neural crest leads to severe cardiovascular defects

NCCs play a critical role in the development of pharyngeal arch arteries (PAAs), and formation of the aortico-pulmonary (AP) septum (Hutson and Kirby, 2003). In combination with other structures, this enables appropriate division of the single vessel that leads from the distal end of the outflow tract, the aortic sac, into separate aortic and pulmonary trunks. When this fails to occur, the single vessel that results is classified as common arterial trunk (CAT) or solitary arterial

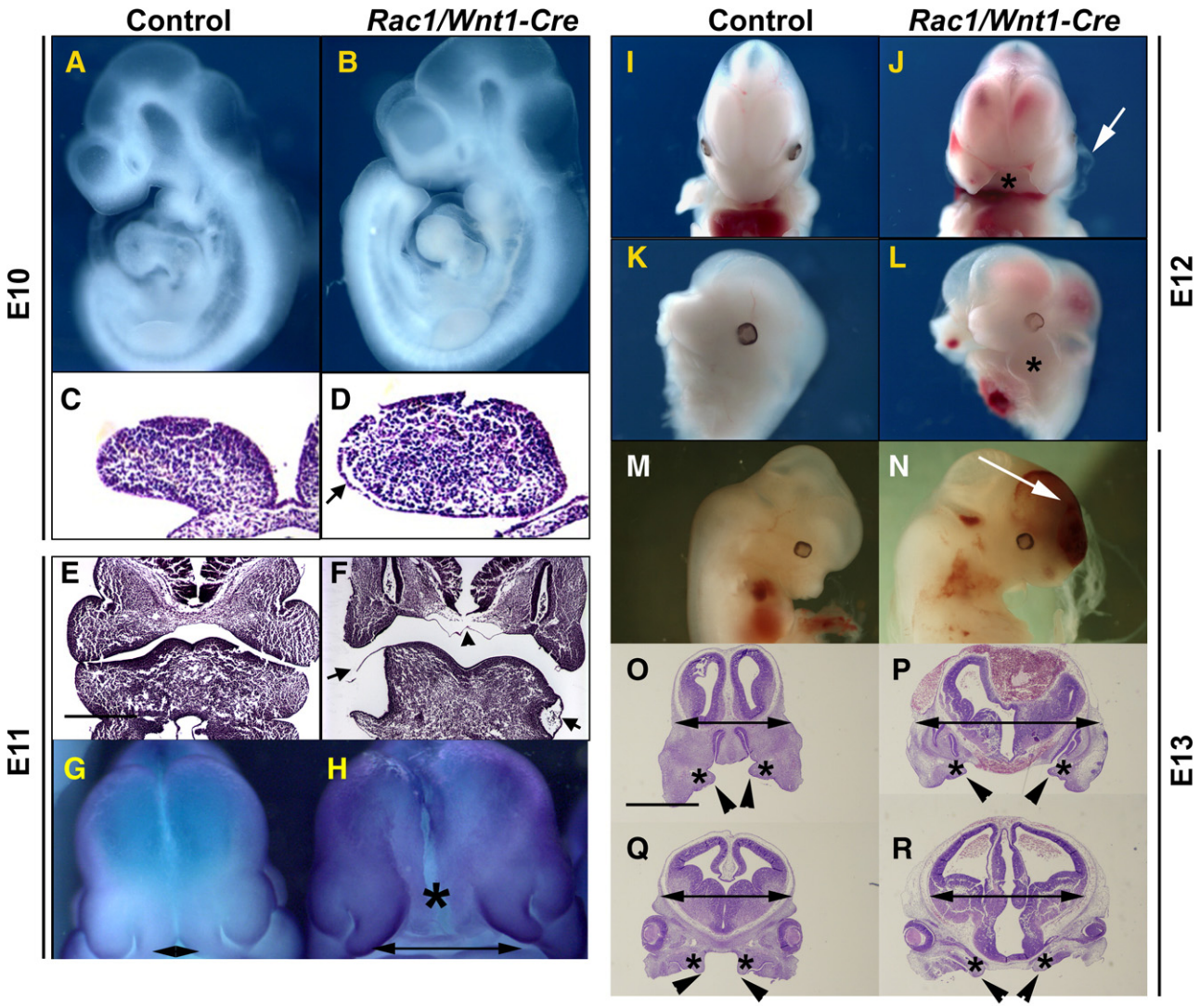

Fig. 1. Craniofacial defects in *Rac1/Wnt1-Cre* mutant embryos. At E10, the *Rac1/Wnt1-Cre* conditional knockout embryo (B) appears superficially unaffected when compared to control (A); however, histological sections show epithelial detachment from the underlying mesenchyme in mutant mandibular arch (arrow in D). At E11 (E–F), mutant embryos have large superficial blisters on mandibular arches (arrows in F). The mutant (H) heads are generally broader than those of controls (G) with a wide separation between the medial nasal processes (double-headed arrows; G, H; in situ hybridization for *Axin-2*). Epithelial detachment can also be seen in the midline region between the two nasal processes (F; arrowhead) corresponding to the position marked by an asterisk in H. At E12, the *Rac1/Wnt1-Cre* mutant embryo has a severe mid-facial cleft (J; asterisk) and rudimentary maxillary processes (L; asterisk). Arrow in J points to an epithelial blister in the first pharyngeal arch. At E13, a mutant (N) shows facial and cranial hemorrhaging (arrow) when compared to a control littermate (M). Histological sections at the level of nasal cavities (O, P) and at eye level (Q, R) show that at E13 the posteror palatal shelves (arrow heads) are much smaller in mutants (R) than in controls (Q) and overall amount of the craniofacial mesenchyme (asterisks in O, P, Q and R) in mutants is reduced. Scale bars indicate 500 μm: F as E; P–R as O.

trunk (SAT); or, more archaically, as 'persistent truncus arteriosus' (PTA).

Our histological examination showed that in all *Rac1/Wnt1-Cre* mutant embryos development of the arterial tree downstream of the heart became increasing abnormal, consistent with a cessation of normal remodelling as well as dysmorphogenesis (Fig. 3). H&E-stained sections of controls at E11 showed septation of the aortic sac was well advanced. PAAs 3, 4 and 6 appeared of similar diameter, PAAs 3 and 4 arising from common paired extensions of the distal aortic sac ('ventral aorta') (Fig. 3A and data not shown). In mutants, the lumen of the aortic sac/ventral aortas appeared enlarged, with only two of the PAA (3 and 6) being continuous to the dorsal aorta (Fig. 3B and data not shown). PAA4 were present but of very small diameter and not always continuously lumenised (Fig. 3S). Pulmonary arteries arose from PAA6 as normal.

By E12, when control embryos had formed separate arterial trunks and a recognizable asymmetric aortic arch structure, the common trunk in mutants connected to dramatically dilated bilateral blood-filled vessels each with a solitary and abrupt connection to an appropriate-sided and more normal-sized dorsal aorta (Figs. 3C–D). The detailed anatomy of the dorsal aortas (data not shown) suggests the dilated vessels connected at a level equivalent to that of PAA3/distal common carotid arteries. Distally, each enlarged vessel also gave rise to a small ventral vessel in a position consistent with this being PAA2. No evidence of separate PAA6/arterial duct or PAA4 vessels could be found by E12. The same abnormalities were found at E13, but the bilateral arterial vessels were even more enlarged, intruding into the ventral body wall of the neck, and pressing against the dense mesenchyme and differentiating cartilage in the tracheal/laryngeal region. The relative diameter of the dorsal aortas to which they connected was even smaller (Figs. 3H, J).

The smooth muscle walls of the great arteries are normally formed by NCCs (Jiang et al., 2000; Nakamura, 1982), whereas those surrounding the dorsal aortas are of mesodermal origin. Like the great arteries of the controls, the aberrant vessels in mutants were also surrounded by wall containing smooth muscle alpha-actin (SMα-A)-positive cells (Figs. 3G–J). Adjacent to the trunk these walls appeared very thick but this is partly due to the plane of sectioning.

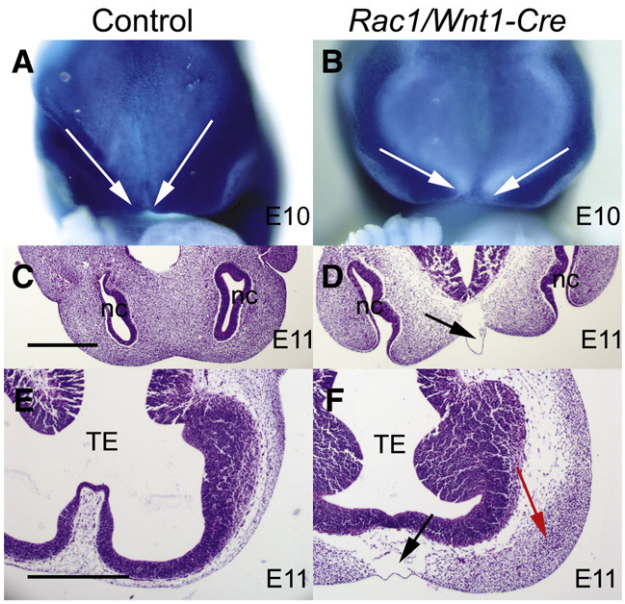

Fig. 2. Early distribution of neural crest-derived craniofacial mesenchyme in *Rac1/Wnt1-Cre* mutants. *R26R* fate determination assay of control (A) and mutant (B) samples at E10. The neural crest (NC)-derived mesenchyme has been visualized by β-galactosidase staining (blue cells in A and B). White arrows in A and B illustrate the more medial NC boundaries in control (A) than mutant (B). Horizontal sections of control (C, E) and *Rac1/Wnt1-Cre* mutants (D, F) show an acellular subepithelial region in the midline at E11 in mutants (black arrows in D and F). A lateral accumulation of mesenchymal cells adjacent to the telencephalon can be seen in *Rac1/Wnt1-Cre* mutants (red arrow in F), but not in controls (E). TE, telencephalon; nc, nasal cavity. Scale bars indicate 500 μm: D as C; F as E.

Although not continuous, SMα-A expression was present around most of these enormous vessels at an (irregular) thickness of up to five cell layers, the latter similar to that of control brachiocephalic and common carotid arteries at E13 (Figs. 3G–J and data not shown). The thickness of the dorsal aorta smooth muscle walls differed little between controls and mutants.

Within the outflow tract (OFT) of the heart itself, abnormalities in the outflow tract cushions of the mutant embryos were demonstrable at E11. Proximally, the endocardially-derived OFT cushions in mutants were of similar structure to those in controls (Figs. 3K, L). More distally, the usual arrangement of two prominent OFT cushions positioned opposite one another across a slit-like lumen was present in controls, so that on their fusion two separate flow routes would be created connecting the outlets of the ventricles to their respective arterial trunks (Fig. 3M). In contrast, the mutants lacked two distinct cushions in this region, cushion tissue had a smaller volume, and was inappropriately positioned on the ventral side of the OFT (Fig. 3N), creating a single off-center flow route. By E12, this single route, connecting to both ventricular apices, was positioned above the right ventricle and led to a single trileaflet valve and thence a single arterial trunk from the posterior/dorsal side of which the pulmonary arteries arose directly (Figs. 3D, F).

Septation of the aortic sac into aortic and pulmonary trunks (AP septation) was well advanced or complete in the control samples at E11, and although the mutant sample contained an AP-septum-like structure (Fig. 3P) reminiscent of control E10 embryos (Fig. 8A), it was too anteriorly positioned and AP septation failed in mutants. This structure contained NCC continuous with other pharyngeal mesenchymal cells (Figs. 5F, H), but simply divided the 'ventral aorta' into left and right compartments (Fig. 3R), not PAA3 and 4 from PAA6.

Control and mutant embryos also differed prominently in that tissue sections of this region in mutant embryos at E11 consistently showed irregular shaped regions of low mesenchymal cell density adjacent to the aortic sac/ventral aorta vessel walls and ventral pharyngeal endoderm (Figs. 3R, S). Such spaces were not found in control embryos (Figs. 3A, Q) and could be distinguished from vessels by their irregular shape and the lack of SMα-A-positive cells around them (Fig. 3S).

To further characterize the differences in aortic sac and PAA structure between controls and mutants, intra-cardiac Indian ink injections were performed at E10 and E11. At E10 development of lumenised PAA4 and 6 was delayed in mutants and PAA3 enlarged. Consistent with our histological findings, arch vessels were of similar diameter to one another in controls at E11 (Fig. 4B) but, although PAA3 and PAA6 were present and patent, the lumen of PAA4 was only of very small diameter in mutants by E11 (Fig. 4D). Whole-mount PECAM-1 immunostaining (Figs. 4E–H), which reveals the extent of endothelial vessel formation even if not fully lumenised, showed the continued predominance of PAA3 at E10.5 in mutants and an already enlarged aortic sac relative to control which remained more aligned with PAA3 than PAA4 in mutant embryos (Figs. 4E, G).

In summary, mutant embryos formed abnormal OFT cushions and exhibited delayed PAA development. The OFT and enlarged aortic sac failed to septate and adjacent pharyngeal mesenchyme developed irregular hypocellular cavities. Instead of the aortic arch and arterial duct arteries, the resulting abnormal single arterial trunk connected to bilateral aneurysmal arterial vessels with incomplete smooth muscle walls that dilated very rapidly between E11 and E12 and continued to dilate if the embryo survived to E13. These vessels each made a single connection to a more normal-sized left or right-sided dorsal aorta at the level of the distal common carotid arteries.

Neural crest cells lacking Rac1 migrate normally in vivo but show defective spreading in vitro

To identify abnormalities in migration of NCCs *in vivo*, we used the *R26R* fate determination assay (Soriano, 1999). Control and mutant whole-mount staining patterns were carefully compared at E9.0 and E10.0. In accordance with the previously published study (Fuchs et al., 2009), we could not detect any evidence of gross differences in NCC migration between these mutant and control samples (Figs. 5A–D). RNA ISH for *Cadherin-6*, also a marker for migrating NCCs, did not demonstrate any significant overall differences in staining pattern either (Suppl. Fig. 4). Concordant with this, we could not detect consistent differences between the most proximal ('upstream') position in the OFT to which NCC had migrated in controls and mutants at E11 (Figs. 5E–H) suggesting that even though NCCs do not enter the distal OFT before E9.5, the OFT septation defect in mutants was not due simply to a failure of any NCC migration deep enough into the heart. Rac1 has a well-documented role in cellular migration *in vitro* (Fukata et al., 2003; Pankov et al., 2005) so we were interested to test the migratory potential of NCCs from neural tubes in 2D culture but since *Rac1*-deficient NCCs failed to migrate from neural tube explants in sufficient numbers we were unable to obtain *Rac1*-deficient NCCs for further study by this route (Supple. Fig. 5A, B).

Since Rac1 has been shown to play an important role in reorganization of the actin cytoskeleton, we tested whether NC-derived cells lacking *Rac1* would spread normally on 2D matrices. We dissected 1st pharyngeal arches from E10 embryos, dissociated them into a single cell suspension and plated the cells onto fibronectin-coated plates. The cultures were harvested after 48 h and stained for β-galactosidase activity (Figs. 6A–B), which demonstrated that more than 80% of cells in both mutant and control cultures were derived from NC. While the control NCCs spread well and formed numerous flat membranous protrusions, the mutant NCCs spread poorly, and had an elongated morphology (Figs. 6C–F). Along with impaired spreading, the mutant cells showed poor attachment. About 80% of control cells, but only about 20% of mutant cells had attached on fibronectin-coated plates after 5 h (data not shown). After 1–3 days in culture, the control and mutant NCCs were stained for f-actin and focal

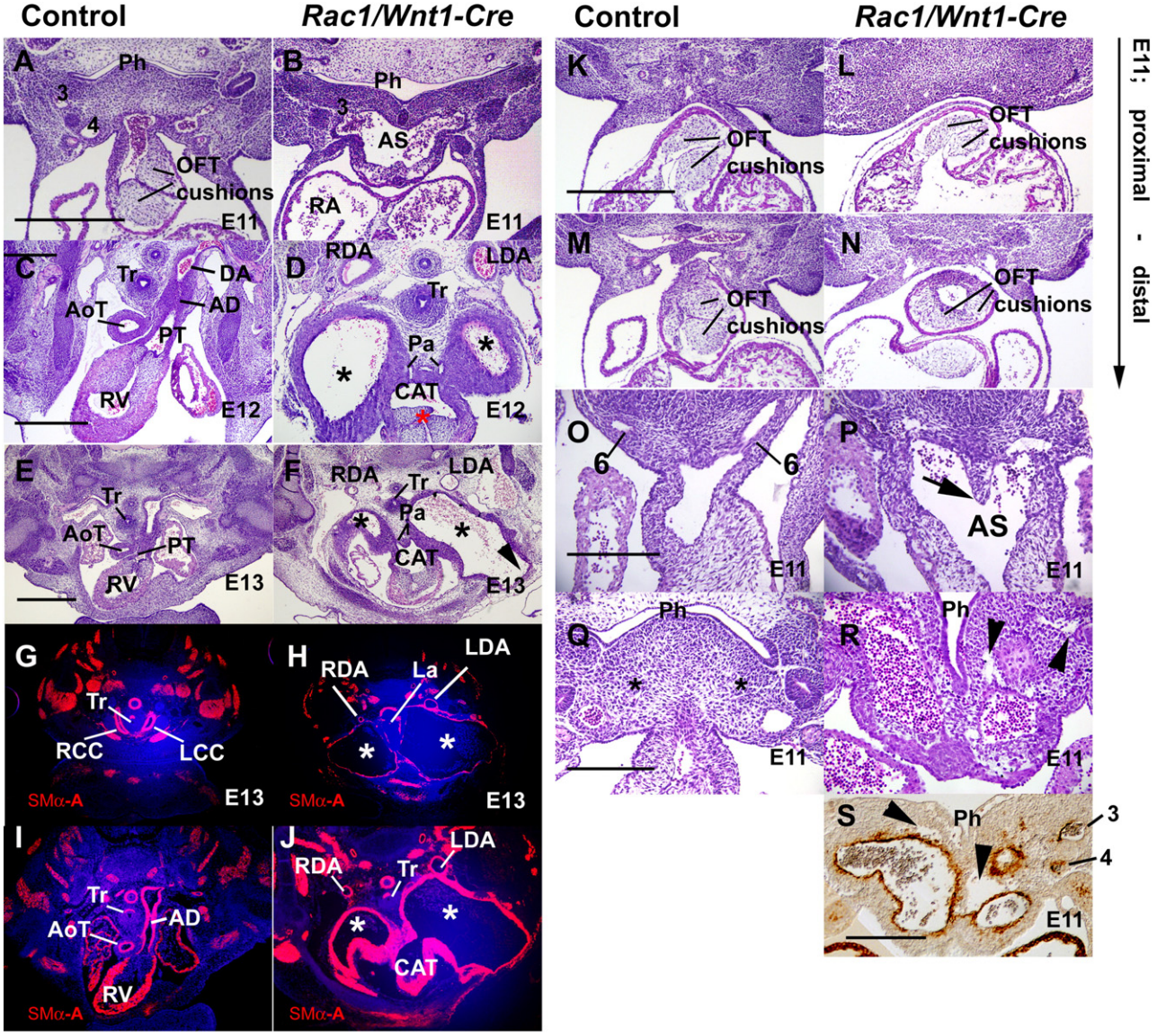

Fig. 3. Pharyngeal arterial and cardiac outflow tract defects in *Rac1/Wnt1-Cre* mutants. A–J; At E11, Outflow tract (OFT) and aortico-pulmonary (AP) septation are in progress and an OFT with well-developed cushions leads to discrete anterior/posteriorly arranged trunk precursors in control (A,) but in mutant (B) a much broader common vessel extends from aortic sac to third pharyngeal arch artery (PAA3). At E12, discrete aortic (AoT) and pulmonary (PT) trunks indicate normal AP septation has occurred in control (C). Only PT connects to pulmonary arteries (below the plane of sectioning) and to the top of the descending aorta (DA) via the arterial duct (AD). In mutant (D) a single three leaflet valve (red asterisk) leads to a large, common arterial trunk (CAT) indicating failure of AP septation, and connects both to pulmonary arteries (Pa) and two dramatically dilated bilateral vessels (*) each of which eventually makes a sole connection to a normal-sized dorsal aorta (left dorsal aorta, LDA; right dorsal aorta, RDA). At E13, the same structures and differences are present in control (E, G, I) and mutant (F, H, J). Smooth muscle α-actin (SMα-A)-positive cells shown in red, nuclei in blue. The mature pattern of great arteries is present in control (G) including right (RCC) and left common carotid (LCC) arteries. In mutant (F, H, J) the abnormal arterial vessels (*) leading from the common trunk are even more dilated, pressing against dense medial mesenchyme around the trachea (Tr) and laryngeal (La) structures and partially interrupting the neck wall (F: arrowhead). They empty only into relatively tiny dorsal aortas (H: LDA, RDA). A high proportion of the abnormal vessel walls contains SM-αA-positive cells, even though the surface area is hundreds of times greater than that of the control arteries. K–P: At E11, the proximal parts of the two OFT cushions are distinct and similarly oriented in both control (K) and mutant (L) embryos. More distally the neural crest (NC)-derived OFT cushions lacking *Rac1* appear fused, smaller and abnormally positioned on the posterior side of the OFT (N) compared to corresponding control cushions (M), creating a single off-center flow route. While AP septation has occurred in the control sample (O; the AP-septum is not a separate structure any more), the mutant sample displays a NC-derived AP-septum-like structure (P; arrow; see also Fig. 5H). Q–S: Mutant pharyngeal mesenchyme contains abnormal irregular cavities (arrowheads in R and S) that are not visible in comparable area of control (Q, asterisk). Cells surrounding these cavities do not stain positive for SMα-A (S). 3, 4, 6: 3rd, 4th, 6th pharyngeal arch arteries respectively; Ph, pharynx. Scale bars indicate either 500 μm (B as A; D as C; F–J as G; L–N as K); or 250 μm (P as O; R as Q; S).

adhesion complexes using FITC-phalloidin and anti-Fak antibodies. Once again, the NC origin was confirmed, this time using immunostaining for β-galactosidase. Control NCCs spread well, forming a large number of focal adhesion complexes and a web-like actin filament network. In contrast, the mutant NCCs displayed very few focal adhesion complexes per cell and few actin filaments all arranged parallel to the long axis of the cell (Figs. 6G–J). Very similar attachment and spreading behaviors, and the same differences between control and mutant genotype cells, were demonstrated whether the cells were plated on fibronectin-, laminin- or collagen-coated dishes. To further examine regulation of cell spreading, control and mutant cells were treated with growth factors. The preparatory serum starvation led to a rapid rounding up of mutant cells while control cells were unaffected (Figs. 6K, L). Subsequent stimulation with EGF and bFGF (100 ng/ml each) induced a detectable increase in spreading (Fig. 6N) suggesting that *Rac1*-deficient cells are at least partially able to respond to growth factor stimulation after serum starvation, although their morphology was still abnormal (Figs. 6K–O).

To conclude, these results demonstrate *Rac1/Wnt1-Cre* NCCs exhibit poor cell attachment and spreading *in vitro*. Defective cell–

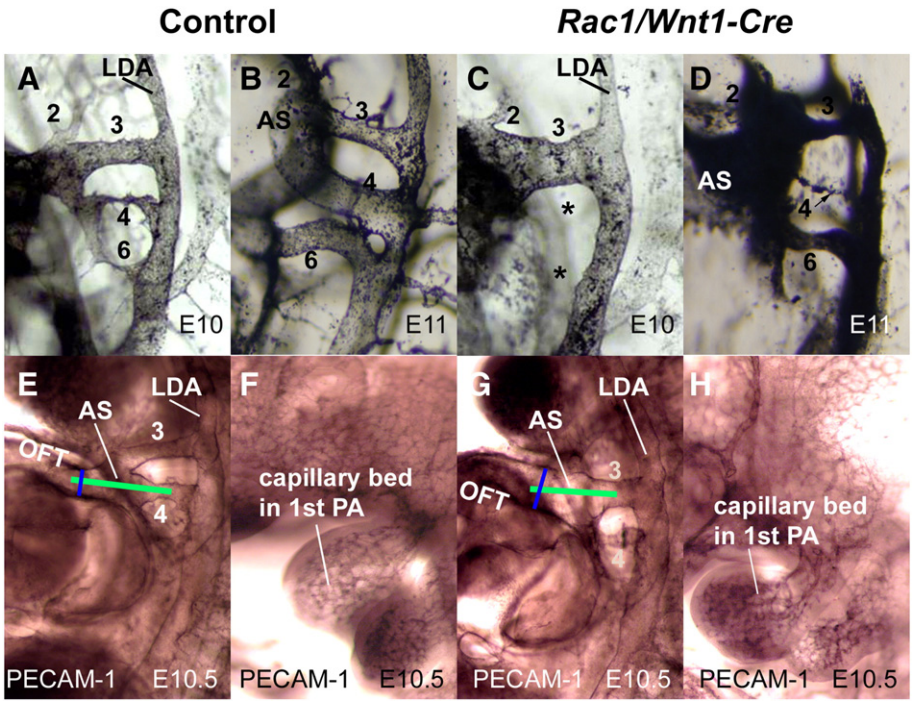

Fig. 4. Abnormal patterning of pharyngeal arch arteries in *Rac1/Wnt1-Cre* mutants. Left lateral view after intra-cardiac ink injection of pharyngeal arch arteries (PAAs) in controls (A, B) and mutants (C, D) at E10 (A, C) and E11 (B, D). All three PAAs; (3, 4, 6) are detectable in control samples (A, B), while in the mutant sample at E10 only a prominent 3rd PAA can be seen. At E11, the mutant displays a prominent 3rd PAA and relatively normal-looking 6th PAA, while the narrow 4th PAA lumen is not completely patent (D). Whole-mount immunostaining for CD31 (PECAM1) at E10.5 showed a wider, abnormally aligned aortic sac in mutant (G) when compared to control (E). Green lines illustrate a difference in alignment between control (E) and mutant (G). Blue lines illustrate diameter of distal OFT. The vascular bed of the first pharyngeal arch in the mutant (H) was similar to that of the control (F) at E10.

matrix interactions could be a common mechanism underlying both these behaviors and the abnormally low mesenchymal cell density in craniofacial and pharyngeal regions observed *in vivo*.

Neural crest cell proliferation, survival and differentiation in Rac1/Wnt1-Cre mutants

Next, we investigated whether the mutant phenotypes observed might be contributed to by deficient cell proliferation or aberrant cell death *in vivo*, by using *BrdU* labelling and phospho-histone 3 immunodetection, and TUNEL staining, respectively. In general, NCC proliferation in mutant and control tissues did not differ at either E10 or E11, stages by which the first observed craniofacial and cardiac phenotypic abnormalities were clearly detectable (Figs. 7A–C, and data not shown). However, consistent with the recent report (Fuchs et al., 2009), we did detect less proliferation of post-migratory NC-derived cells in mutant embryos at E13 (Figs. 7D–E).

A strikingly higher incidence of cell death was detectable in the largely NC-derived pharyngeal mesenchymal cells surrounding the aberrant aortic sac and arch vessels in *Rac1/Wnt1-Cre* mutants relative to controls at E11 (Figs. 7H–K). Although the incidence was less, we detected more than twice the percentage of apoptotic cells in the hypocellular craniofacial midline region at E11 in mutants as in controls (Figs. 7F, G; data not shown). However, we could not consistently associate the large blisters in lateral aspects of the mandibular arch with elevated levels of apoptosis (data not shown).

We also made a careful comparison of NCC shape in the OFT cushions of control and mutant embryos at E11, and demonstrated that NC-derived control cells more often appeared elongated (had longer cellular processes) than *Rac1*-deficient cells which were more often rounder due to shorter or absent processes (Figs. 7L–M). Similar rounded cells were not detected in other mesenchymal regions known to be populated by NC-derived cells.

In addition to the craniofacial mesenchyme, OFT and AP septation, stability of PAAs, and SMC formation, cranial NCCs also contribute to development of afferent neurons and glial cells of the cranial ganglia (Barlow, 2002; Kalcheim and Le Douarin, 1986; LeDouarin, 1982). We therefore examined the morphology of cranial ganglia in *Rac1/Wnt1-Cre* embryos by whole-mount immunohistochemistry with anti-neurofilament antibody at E11. In all mutant samples, the trigeminal ganglia were reduced in size, the superior cervical ganglia (III) disorganized, and the oculomotor nerves missing. The glossopharyngeal nerve (IX) branched from vagal nerve (X) in an aberrant combined structure. The expression pattern of *Sox10* in *Rac1/Wnt1-Cre* mutants confirmed their smaller trigeminal ganglia relative to those in controls (Suppl. Fig. 6).

As cardiac cranial NCCs have important roles in OFT/AP septation and smooth muscle wall formation, and mutant embryos had defects in these structures and processes, we examined muscle differentiation in this region more closely. NCCs are thought to regulate septation in part by influencing the migration of adjacent secondary heart field cells into the distal OFT wall of the heart (Waldo et al., 2005a; Yelbuz et al., 2002). Normally, a myocardial sleeve is formed as far as the reflection of the pericardium/body wall at the distal end of the OFT at E10 and such a pattern was indeed detected in sections of control hearts using MF20 antibody staining (Fig. 8A). In mutant structures, the most distal part of the sleeve was not MF20-positive, and a disconnected population of MF20-positive cells was present between the endothelium and outflow tract wall adjacent to the aortic sac (Fig. 8B) suggesting that *Rac1*-deficient NCCs were unable to perform their normal role. A day later, secondary heart field cells and cranial NC start to differentiate into smooth muscle cells of the OFT valves, trunks and great arteries downstream of the heart in a distinctive pattern (Brown and Baldwin, 2006). To examine the initiation and distribution of differentiating smooth muscle cells in this region, SMα-A antibody staining was performed on sections at E11. There were no striking differences in overall intensity or pattern of staining

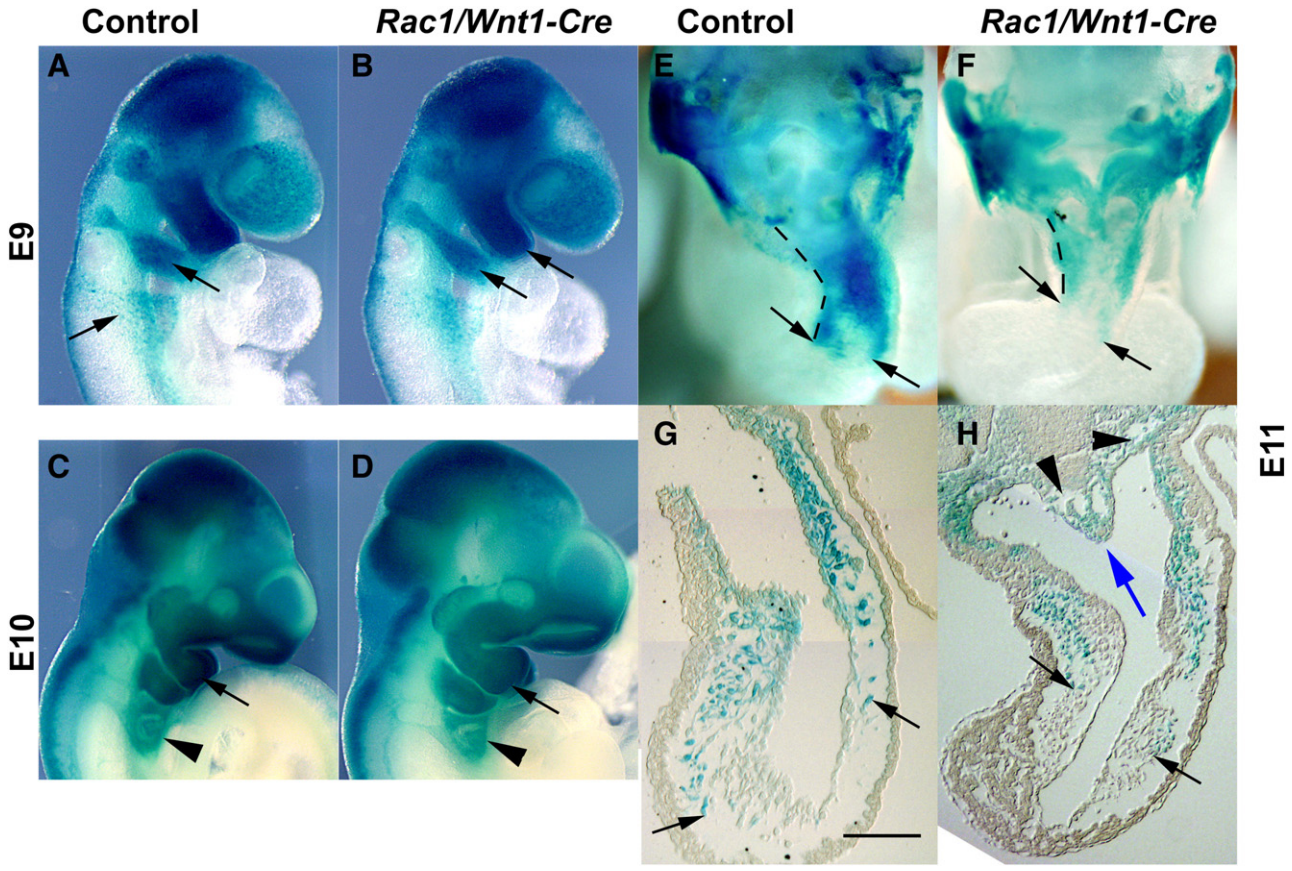

Fig. 5. Neural crest cells deficient in *Rac1* migrate normally in vivo. Lineage tracing of migrating neural crest cells (NCCs) using whole-mount *R26R* fate determination assay at E9 (A, B), E10 (C, D) and E11 (E–H). A–D: External lateral views of control (A, C) and mutant embryos (B, D) show identical staining patterns, including at the level of pharyngeal arches 4–6 (arrowheads); E–F: whole-mount embryos dissected transversely at the outflow tract (OFT) level, and sections, demonstrating cardiac NCC migration into the OFT has occurred to the same morphological position in control (E, G) and mutant (F, H) embryos (black arrows point to most proximally migrated positively staining (blue) NC-derived cells; blue arrow points to an aortico-pulmonary septum-like structure containing blue NCCs; black arrowheads point to aberrant mesenchymal cavities). Hatched lines depict the length of the OFT (E, F). Scale bar indicates 100 μm (H as G).

between mutants and controls in the aortic sac and arch vessel wall cells but the SMα-A-positive cells forming the smooth muscle cell layers in mutants appeared less tightly packed, and present in more (disorganized) layers, thus failing to form as compact a layer around the endothelial lining of the aortic sac region as seen in controls (Figs. 8C–D). Expression of SMα-A *per se* is only a crude measure of smooth muscle cell differentiation and it has been shown by others (Wang et al., 2004) that the degree of normal 'contractile' smooth muscle differentiation is controlled by a balance between myocd (myocardin, a smooth muscle-specific transcriptional co-activator of serum response factor) and activated Elk1 (a member of the Ets family of transcription factors). Consistent with relatively strong SMα-A staining levels in mutant SMCs, we could not detect any increase in the level of phosphorylation of Elk1 in *Rac1/Wnt1-Cre* mutants when compared to controls (data not shown) suggesting that a lack of *Rac1* does not affect the molecular switch regulating this aspect of differentiation and would not contribute to the abnormal organization.

We also examined a different aspect of differentiation, the organization of smooth muscle cell contractile apparatus, by transmission electron microscopy. Semi-organized filamentous actin bundles ('hairy actin') were identified in about 50% of the smooth muscle cells adjacent to distal aortic sac-derived vessels examined in controls at E11 ($n=10$) (Fig. 8E) but despite intensive screening similar subcellular structures could not be found around mutant vessels (Fig. 8F) where cells appeared to be simply of a 'secretory' fibroblast phenotype, even though they were clearly located in the region where most cells were SMα-A-positive. Organized actin structures were present in cells immediately adjacent to the endothelial cells of dorsal aortas in both mutant and control samples (data not shown), consistent with the smooth muscle cells here not being of NC origin so not genotypically altered in mutant embryos. Thus mutant cardiac NC-derived cells around the arterial structures immediately distal to the heart differ in at least two respects from their control counterparts. Overall, post-migratory *Rac1*-deficient NCCs in this region in mutants exhibited areas of defective cell proliferation, cell survival, organization and differentiation.

In summary, these analyses imply that *Rac1* is required in cranial NCCs for appropriate differentiation and morphogenesis of post-migratory NCCs and adjacent cells including frontonasal and pharyngeal arch mesenchyme, secondary heart field cells, smooth muscle cells, OFT cushion mesenchymal cells and cranial nerves. *In vitro*, *Rac1*-deficient NCCs were defective in cell–matrix interactions, cell attachment and spreading. Related defective mechanisms might also underlie the examples of regionalized abnormally low mesenchymal cell density, abnormal cell shape or higher incidence of cell death coincident with or precedent to the abnormalities in the developmental events *in vivo* listed above in *Rac1/Wnt1-Cre* mutants.

Discussion

In this study, we have analyzed the role of *Rac1* in neural crest cells (NCCs) during mouse embryogenesis by deleting *Rac1* gene expression in NCCs with *Wnt1-Cre*. Our results show that *Rac1* in NCCs is required for normal craniofacial and cardiovascular development. Mutant (*Rac1/Wnt1-Cre*) embryos consistently died during the

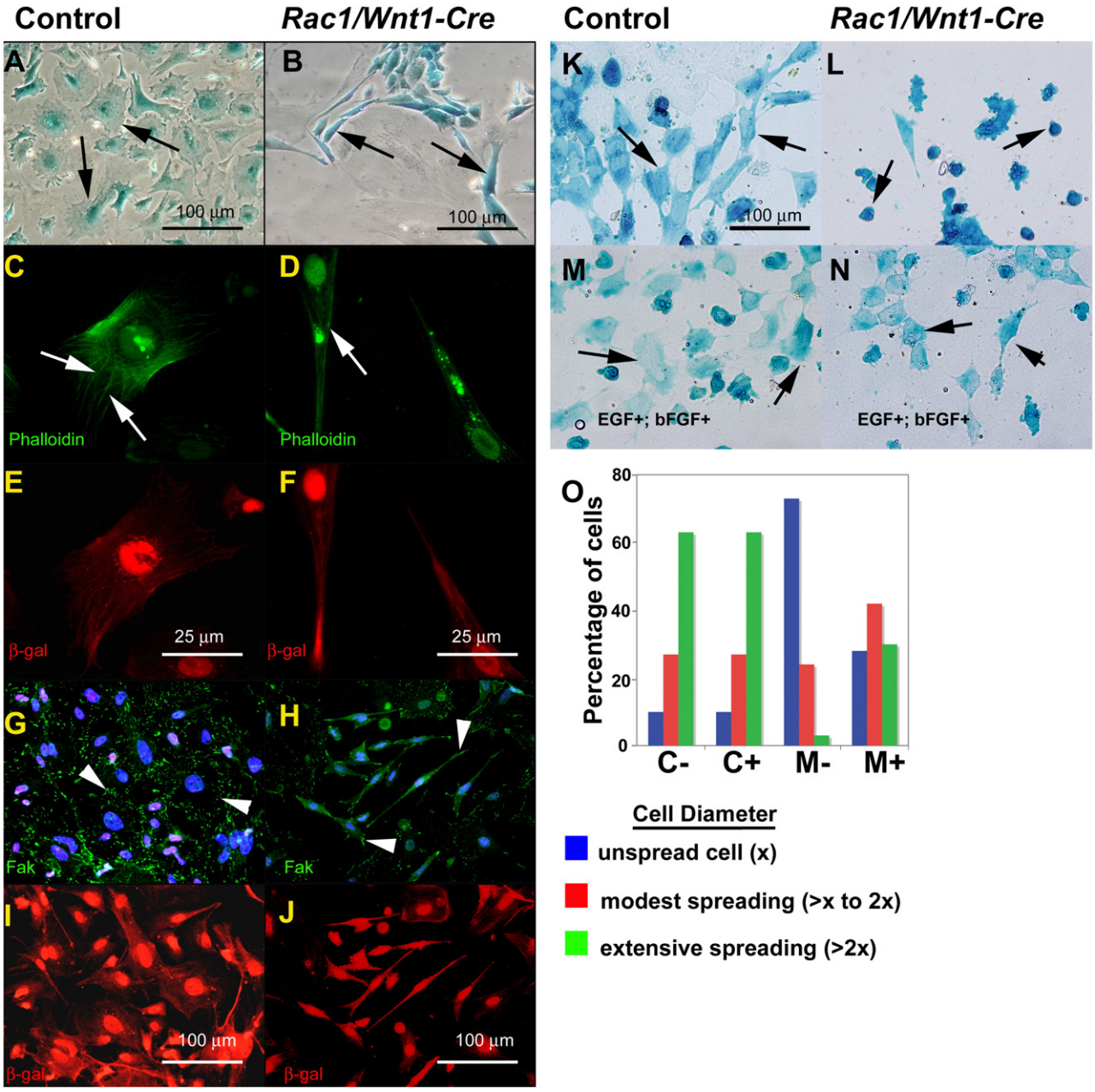

Fig. 6. *Wnt1-Cre*-induced recombination of *Rac1* impairs neural crest cell spreading on 2D matrices. *Rac1*-deficient neural crest (NC)-derived pharyngeal arch mesenchymal cell cultures (B, D, F, H, J) showed reduced spreading, aberrant clumping (B), elongated phenotype and reduced number of focal adhesion complexes on fibronectin when compared to corresponding control cultures (A, C, E, G, I). A, B, *R26R* fate determination assay, arrows point to positively stained NC-derived cells; C–D, phalloidin staining, arrows point to actin stress fibers; G, H, immunostaining for Fak, white arrowheads point to positively staining focal adhesion complexes; E, F, I, J, immunostaining for β-galactosidase. After serum starvation, most of the *Rac1*-deficient cells showed a rounded phenotype (L; arrows point to rounded cells) when compared to corresponding control cells (K; arrows point to well-spread cells). Growth factor stimulation with epidermal growth factor (EGF; 100 ng/ml) and basic FGF (bFGF; 100 ng/ml) induced moderate cell spreading in mutants (arrows in N), although still remains less than in that in corresponding controls (M; arrows point to spread cells). Bar chart (O) shows quantification of changes in cell spreading after stimulation with EGF and bFGF (100 ng/ml each). Based on the diameter of an unspread cell (x), cells were divided into three groups: no spreading (blue column), modest spreading: >x to 2x (red column); extensive spreading: >2x (green column) and the percentage of cells in each group calculated. More than 200 cells were scored in each group. Scale bars indicate either 100 µm (A, B; G as I; J as H; L, M, N as K) or 25 µm (C as E; D as F).

twelfth embryonic day with cleft face, grossly malformed cardiac outflow tract and great arteries and extensive areas of epithelial attachment in the craniofacial and pharyngeal region. In this report we present evidence that *Rac1*-dependent patterning, cell spreading, survival, proliferation and differentiation contribute to these phenotypic features.

A recent paper from Fuchs et al. reports an analysis of mice of a very similar mutant genotype (Fuchs et al., 2009). The phenotypic features described in our present study are summarized and compared with those of Fuchs et al. (2009) in Table 1, and are considered in greater detail elsewhere in this Discussion. The broad phenotypes of *Rac1*/*Wnt1-Cre* mutants described by Fuchs et al. (2009) are consistent with their hypothesis that loss of *Rac1* leads to a depletion of the neural crest pool due to its failure to proliferate in response to EGF. While our findings are in full agreement with the statement that post-migratory NC-derived cells deficient in *Rac1* fail to proliferate normally, some of the defects, particularly the epithelial detachment and associated mesenchymal cavity formation, occur earlier than the first detectable abnormalities in cell proliferation. This, together with the fact that other NC-specific mutants which

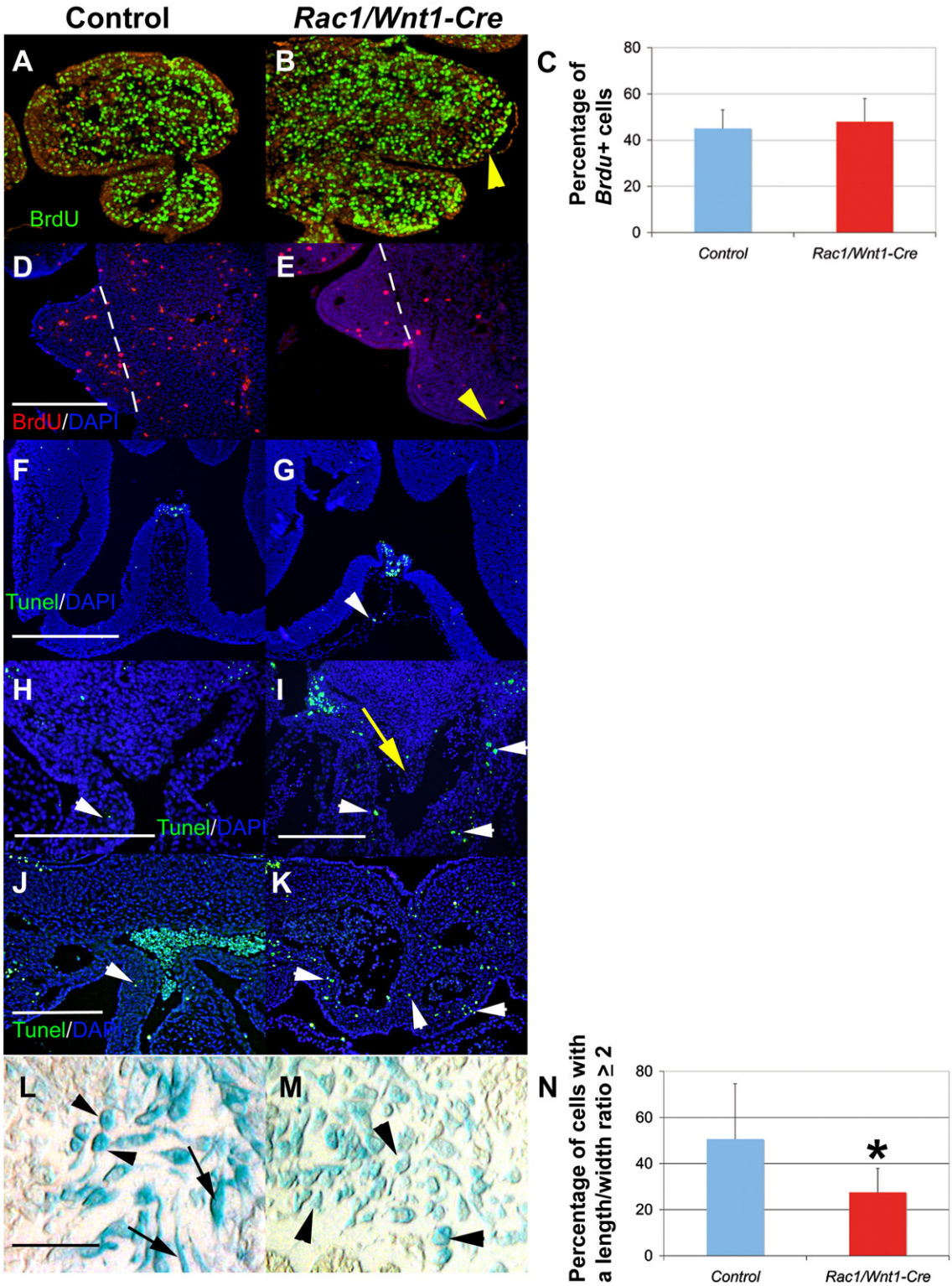

Fig. 7. Effect of *Rac1* inactivation in neural crest cells on cell proliferation, apoptosis and cellular morphology *in vivo*. A–C, *BrdU* incorporation assay to assess mesenchymal cell proliferation in the first and second pharyngeal arches at E10. *BrdU*-labelled nuclei green, counterstain red (A, control; B, mutant). Bar chart in C shows the quantification as a percentage of *BrdU*-positive cells; blue column, control; red column, *Rac1/Wnt1-Cre* mutant; error bars depict standard deviation ($n=3$). D–E: Cell proliferation is dramatically reduced in *Rac1*-deficient neural crest (NC)-derived palatal mesenchyme at E13 (E) relative to control (D) (*BrdU* incorporation assay: *BrdU*-labelled nuclei red, (white arrowheads), counterstain DAPI blue; D, control; E, mutant). Yellow arrowheads in B and E point to sites of epithelial detachment, hatched lines in D and E define the lateral boarder of the palatal shelf mesenchyme. F–G: TUNEL staining (green; counterstain DAPI blue) of the midline frontal craniofacial region showing signal in the highly hypocellular NC-derived mesenchyme of a *Rac1/Wnt1-Cre* mutant sample (G, white arrowhead) compared to a corresponding control specimen (F). H–K: TUNEL staining (green; counterstain DAPI blue) in the largely NC-derived mesenchyme surrounding distal outflow tract (OFT) and abnormal downstream vessels (white arrowheads in I, K) and also in the AP-septum-like structure (yellow arrow in I) shows more apoptosis in *Rac1/Wnt1-Cre* mutants when compared to equivalent regions in controls (white arrowheads in H and J). L–N: NC-derived OFT cushion mesenchymal cells (blue: *R26R* fate determination assay; black arrows) in *Rac1/Wnt1-Cre* mutants (M) appear more often rounder, with shorter cellular projections, than the corresponding control cells (L). Black arrows (L) point to elongated cells; black arrowheads (L, M) point to round cells. Bar chart (N) shows quantification of the cell shape differences: Percentage of cells with a length:width ratio ≥2 shown for controls (blue column) and mutants (red column); error bars show standard deviation ($n=3$); *$p<0.05$ (Wilcoxon rank sum test). Scale bars indicate 250 μm in D and H–L, and 500 μm in F (E as D; I as J; G as F).

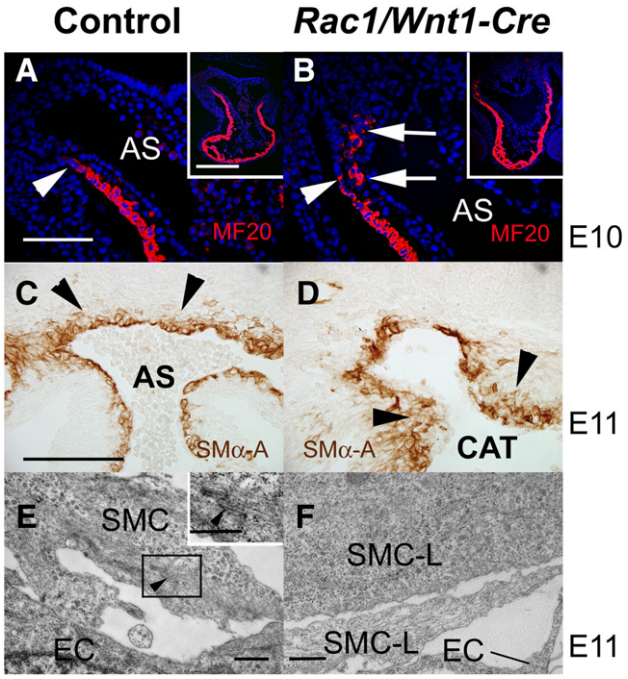

Fig. 8. Abnormal outflow tract and vessel wall differentiation in *Rac1/Wnt1-Cre* mutants. Immunostaining for MF20 in distal outflow tract (OFT) of control E10 heart (A) shows a continuous sleeve of expression to the body wall reflection (white arrowhead) but in mutant (B) MF20-expressing cells are aberrantly located (white arrows). Low power images shown in insets (A, B). At E11, neural crest cells (NCCs) deficient in *Rac1* (D) immunostained for smooth muscle α-actin (SMα-A) form a more extensive and irregular layer (arrow heads) around the proximal arterial vessels than those in controls (C). E, F: Transmission electron micrographs of putative smooth muscle cells adjacent to endothelial cells in a position slightly distal to one such as in C, D. Distinctive semi-organized f-actin bundles shown in inset E (black arrowhead) could be found in many control cells but none of the mutant cells (F) examined. AS, aortic sac; CAT, common arterial trunk; SMC, smooth muscle cell; SMC-L, SMC-like cell in mutant; EC, endothelial cell. Scale bars indicate either 250 μm (B as A), 200 μm (D as C) or 500 μm (E and inset, F).

display insufficient numbers of NCCs do not demonstrate similar defects in epithelial attachment or mesenchymal condensation (Chen et al., 2007; Ko et al., 2007), suggests that factors other than reduced size of the NC pool contribute to some of the phenotypes we report here. As the genetic approach used by Fuchs et al. and us are so similar, what might cause the striking differences in the resulting phenotypes? Both studies used the same very well validated *Wnt1-Cre* driver line, but the design of the responder line (floxed *Rac1*) is a possible candidate: in our mutants exon1 of the *Rac1* gene was floxed (flanked by *loxP* sites), while exon 3 was floxed in those studied by Fuchs et al. This subtle difference might lead to minor disparities in efficiency and or timing of early recombination which, in turn, could lead to a much more substantial divergence in early phenotypes.

Table 1
Phenotypic comparison of *Rac1/Wnt1-Cre* mutant embryos between the present study and that of Fuchs et al. (2009).

Phenotype	Present study	Fuchs et al. 2009
Lethality	By E12.0	From E13.5
NCC migration *in vivo*	Grossly normal	Grossly normal
Cleft face	Yes	Yes
Epithelial detachment	Yes, detectable at E10.0	Not reported
Mesenchymal acellular cavities	Yes, detectable at E11.0	Not reported
Reduced proliferation of post-migratory NCCs	Yes, detectable at E11.5	Yes, detectable at E11.5
AP septation defect	Yes	Yes
Abnormal arch artery development	Yes	Not reported
Elevated apoptosis in post-migratory NCCs	Some regions by E11.0	Not detected
NCC migration from neural tube explant, (2D, *in vitro*)	Defective	Normal
Post-migratory NCC spreading (on 2D matrix *in vitro*)	Defective[a]	No abnormalities reported

AP aortico-pulmonary; NCC neural crest cell.
[a] Post-migratory NCCs derived from the first pharyngeal arch.

Rac1 deficiency, cell morphology and neural crest cell migration

Rac1 has been shown to play an instrumental role in epithelial and mesenchymal cell polarization, and in cell migration *in vitro* and *in vivo* (Schmitz et al., 2000). In particular, Rac activation at the leading edge has been shown to be a key event for directional migration (Grande-Garcia et al., 2005; Nishiya et al., 2005), and a precise level of Rac1 signaling is required for persistent directional migration, which is then maintained by numerous feedback loops (De Calisto et al., 2005; Ridley et al., 2003; Wallingford, 2005). Therefore, the degree of apparently normal migration of *Rac1*-deficient NCCs *in vivo*, as shown previously (Fuchs et al., 2009) and confirmed by the present study, is quite remarkable. How can these *in vitro* results and our *in vivo* results be reconciled? One major difference is that cells migrating *in vivo* will often be responding to three-dimensional cues and conditions, whether with matrix or other cells. Matrix composition *in vivo* is complex and dynamic and has yet to be fully described. There is currently no satisfactory three-dimensional *in vitro* culture system in which to study onset and early NCC migration so this aspect must remain unresolved.

Despite apparently normal NCC migration *in vivo*, and consistent with the expected phenotype, *Rac1*-deficient NC-derived cell cultures showed poor plating efficiency, aberrant clumping, reduced spreading and long narrow cell shape associated with fewer, parallel stress fibers and a reduced number of focal adhesion complexes. This phenotype is very similar to that of *Rac1*-deficient embryonic fibroblasts (Guo et al., 2006) and of non-migratory cells with very low Rac1 activity (Pankov et al., 2005), and is consistent with the observed *in vivo* mesenchymal phenotypes of abnormally low cell density often associated with detached epithelium (in several locations), and abnormal cell morphology (in OFT cushions).

Epithelial blisters, mesenchymal cavities, and mid-facial clefting

Deletion of *Rac1* in the NC leads to embryonic lethality during mid-gestation with defects in craniofacial structures, cardiac outflow tract and pharyngeal vessels. A consistent early and novel phenotype of *Rac1* mutant embryos is acellular or hypocellular regions between epithelia and mesenchymal cells (blistering) or within mesenchyme (irregular cavities), which was detectable as early as E10. It should be noted that reduced proliferation was observed in post-migratory NCCs only much later (≥E11.5) and thus it is unlikely that the observed phenotypes would be caused by inability of NC-derived cells to respond to mitogenic stimuli.

Blistering was always first detected on the lateral aspects of the mandibular arch, but occurred later at other sites in which the underlying mesenchyme is populated by NC-derived cells. These included the maxillary processes, craniofacial midline and posterior pharyngeal mesenchyme. The blisters and hypocellular regions in the craniofacial mesenchyme and posterior pharyngeal mesenchyme were associated with increased cell death. However, an occurrence of apoptotic cells was not strictly limited to the immediate vicinity of hypocellular or blister regions; Instead, they were relatively broadly spread through the NC-derived mesenchyme in these areas. Based on these findings, and in conjunction with a previous published report demonstrating that in an unrelated NC-specific mutant a dramatic increase in the level of apoptosis in post-migratory NCCs did not lead to a similar formation of hypocellular regions (Wang et al., 2006), we conclude that, while increased apoptosis is likely to be an important contributory factor to the observed phenotypes, other mechanisms

such as reduced cell–matrix or cell–cell interactions will play a role in their initiation, and subsequently.

Despite the enormous size and degree of epithelial detachment in the blisters there, the lower jaw developed relatively normally. In contrast, the upper jaw became severely malformed as mutant embryos developed a mid-facial cleft by E12. A direct role for lateral blistering in this seems unlikely. Instead, the epithelial blistering and adjacent hypocellular mesenchyme we observed in the facial midline at E11 is strongly implicated as a key marker of embryos in which mid-facial fusion will fail and perhaps part of the underlying mechanism. The same feature was considered instrumental previously in the mid-facial clefting in mice exposed to the teratogenic amino acid analogue diazo-oxo-norleucine (DON) at E11 (Burk and Sadler, 1983). DON-treated embryos also display wide separation of medial nasal processes and abnormal widening of the anterior face and head, closely resembling those seen in *Rac1*/*Wnt1-Cre* embryos, along with larger lateral accumulations of NCC. This implies that the mid-face clefts seen in *Rac1* mutants result from an abnormal distribution of post-migratory NC-derived craniofacial mesenchyme during facial development, one result of which is mesenchymal hypocellularity and epithelial blistering in the midline.

Cardiac outflow tract and pharyngeal defects in Rac1/Wnt1-Cre mutants

Rac1/*Wnt1-Cre* mutants display aberrant patterning of pharyngeal arch arteries, followed by common arterial trunk ('persistent truncus arteriosus') and highly aneurysmal bilateral distal pharyngeal arteries. It was recently suggested that an adequate number of NCCs is required for the normal architecture of the aortic sac, and stabilization of nascent posterior PAAs 4 and 6, which in turn is required for appropriate AP septation (Bradshaw et al., 2009). Thus, it is possible that despite seemingly normal NCC migration, the observed defects in great artery development result from a reduced number and/or other aspect of behaviour of NCC adjacent to developing PAAs 4 and 6. *Rac1*-deficient NC-derived pharyngeal mesenchyme also develops aberrant cavities, around the aortic sac and ventral aorta, clearly detectable at E11. These cavities lie immediately adjacent to, and precede the most acute dilation phase of, the abnormal arterial vessels, making it likely that an inadequate quantity of extra-arterial mesenchyme contributes to the formation of the aneurysmal vessel phenotype present by E12. Details of later anatomy suggest that the aberrant great arterial vessels in mutants are derived largely from ventral aorta, again consistent with the location of hypocellular mesenchyme at E11.

Although a number of models with abnormal neural crest genotypes display OFT and AP septation failure and a common arterial trunk, the development of extremely dilated arterial vessels downstream of this distinguishes our model from many other NC-specific mutant phenotypes. However, a severely dilated arterial trunk phenotype is present in NC-specific *Pinch1* mutants (Liang et al., 2007) very similar to that seen in our *Rac1*-deficient model. Pinch1 is a LIM domain containing adapter protein that has been shown to mediate integrin/integrin-linked kinase-dependent signaling (Clark et al., 2003; Hobert et al., 1999). Previous studies have implicated *Rac1* in integrin-mediated cell matrix interactions and suggested that loss of *Rac1* leads to *anoikis* (Guo et al., 2006), which may contribute to the hypo- and acellular mesenchymal phenotype seen in this study especially the aortic sac-adjacent pharyngeal mesenchyme in which more apoptosis was most clearly detectable. Since numerous studies have implicated Rac1 in integrin signaling (Nishiya et al., 2005; Ridley et al., 2003; Rose et al., 2007), it is tempting to speculate that in cardiac NCCs both Rac1 and Pinch1 interact with the same integrin signaling pathway to regulate critical cell–matrix interactions. Integrins are major receptors for ECM molecules but are molecularly highly varied (Giancotti and Ruoslahti, 1999). Little is known about precisely which ones regulate these aspects of development in NCCs other than that β1 integrins, which represent the largest subfamily of β integrins, are not essential for migration or septation (Breau et al., 2009). In contrast, a recent report showed that focal adhesion kinase (*Fak*), which is activated by integrin signaling, plays a critical role in OFT septation (Vallejo-Illarramendi et al., 2009). While the overall cardiac phenotype of *Fak*/*Wnt1-Cre* mutants appeared milder than that of corresponding *Rac1* mutants, the *Fak*-deficient OFT cushion mesenchymal cells displayed an aberrant rounded morphology, which appeared very similar to that seen in our *Rac1*/*Wnt1-Cre* mutants. A relationship between Fak and Rac1 is further supported by our findings that immunostaining of cultured NC-derived pharyngeal arch cells showed a markedly reduced pattern of Fak in focal adhesion complexes although the total amount of Fak1 protein measured in cell lysates was not affected (data not shown). This is consistent with the work by Guo et al. (2006) showing that Rac1 deletion greatly reduced the number and size of focal adhesion complexes in mouse embryonic fibroblasts (MEFs) but not the expression of focal adhesion complex components. Another similarity between *Rac1*-deficient NC-derived cells and MEFs is their inability to respond to EGF stimulation (Fuchs et al., 2009; Guo et al., 2006), while stimulation of NC-derived cells with bFGF led to enhanced spreading (present study) or increased proliferation (Fuchs et al., 2009).

The rounded cell shape of most of the NCC cells that populate the OFT cushions may contribute to the abnormal morphology (shape, reduced volume) of these cushions in mutants. A higher incidence of apoptosis in OFT mesenchyme in mutants was not detected.

As well as defects in arch artery formation and stability, failure of OFT and aortico-pulmonary septation, other mouse models also have a somewhat shortened, very straight, rather symmetrical outflow tract, and aberrantly located striated myosin-expressing cells adjacent to an enlarged aortic sac (Bradshaw et al., 2009) that we observe in *Rac1* mutants. In particular, these features are consistent with those of Splotch$^{2H/2H}$, attributed to the failure of NCC to regulate the location and differentiation of secondary heart field (SHF) cells at the distal end of the OFT appropriately (Bradshaw et al., 2009). SHF cells contribute not only to myocardium but also smooth muscle of the arterial trunks (Waldo et al., 2005b) so the abnormal smooth muscle-α-actin-positive cell wall around the aortic sac and ventral aorta in *Rac1*/*Wnt1-Cre* mutants could also be a consequence of this.

Other mouse models with common arterial trunk (CAT) frequently survive to birth, but rarely have such dysmorphic arteries. Whatever the functionality of the smooth muscle wall of these abnormal vessels, given their shape and large volume they are unlikely to behave as normal arteries hemodynamically, compromising the supply of oxygen and nutrients to all other tissues even in those embryos that survive such a sudden expansion of arterial volume as occurs between E11 and E12. Indeed, the occasional survivors to E12 may represent those where the expansion was less severe. Embryos lacking *Pinch1* in NCCs have a similar great artery phenotype but survive to birth (Liang et al., 2007), consistent with Rac1 not being simply a downstream mediator of Pinch1-dependent functions.

In conclusion, our results demonstrate that Rac1 plays a critical role in early post-migratory NCCs. Failure of Rac1 signaling leads to the localized formation of aberrant epithelial blisters and mesenchymal cavities in craniofacial and pharyngeal tissues which are sometimes accompanied by apoptosis, thereby disrupting major morphological events including facial midline fusion, OFT and AP septation and great artery remodelling. Given the complexity of Rac1-mediated signaling, future studies will be needed to clarify the roles of various Rac1-regulated pathways in cardiac and craniofacial development.

Acknowledgments

We thank Saverio Bellusci, Robert Maxson and Stijn DeLanghe for in situ hybridization probes, DSHB for the NF-20 antibody, and Dorothy Sorenson for interpretation of TEM images. This study was financially supported by NIH RO1 DE013085 and HL074862 (to VK).

Appendix A. Supplementary data

Supplementary data associated with this article can be found, in the online version, at doi:10.1016/j.ydbio.2010.02.021.

References

Aznar, S., Lacal, J.C., 2001. Rho signals to cell growth and apoptosis. Cancer Lett. 165, 1–10.

Barlow, L.A., 2002. Cranial nerve development: placodal neurons ride the crest. Curr. Biol. 12, R171–R173.

Bradshaw, L., Chaudhry, B., Hildreth, V., Webb, S., Henderson, D.J., 2009. Dual role for neural crest cells during outflow tract septation in the neural crest-deficient mutant Splotch(2H). J. Anat. 214, 245–257.

Breau, M.A., Dahmani, A., Broders-Bondon, F., Thiery, J.P., Dufour, S., 2009. {beta}1 integrins are required for the invasion of the caecum and proximal hindgut by enteric neural crest cells. Development 136, 2791–2801.

Brown, C.B., Baldwin, H.S., 2006. Neural crest contribution to the cardiovascular system. Adv. Exp. Med. Biol. 589, 134–154.

Burk, D., Sadler, T.W., 1983. Morphogenesis of median facial clefts in mice treated with diazo-oxo-norleucine (DON). Teratology 27, 385–394.

Chai, Y., Jiang, X., Ito, Y., Bringas Jr., P., Han, J., Rowitch, D.H., Soriano, P., McMahon, A.P., Sucov, H.M., 2000. Fate of the mammalian cranial neural crest during tooth and mandibular morphogenesis. Development 127, 1671–1679.

Chen, Y.H., Ishii, M., Sun, J., Sucov, H.M., Maxson Jr., R.E., 2007. Msx1 and Msx2 regulate survival of secondary heart field precursors and post-migratory proliferation of cardiac neural crest in the outflow tract. Dev. Biol. 308, 421–437.

Clark, K.A., McGrail, M., Beckerle, M.C., 2003. Analysis of PINCH function in Drosophila demonstrates its requirement in integrin-dependent cellular processes. Development 130, 2611–2621.

Creazzo, T.L., Godt, R.E., Leatherbury, L., Conway, S.J., Kirby, M.L., 1998. Role of cardiac neural crest cells in cardiovascular development. Annu. Rev. Physiol. 60, 267–286.

Danielian, P.S., Muccino, D., Rowitch, D.H., Michael, S.K., McMahon, A.P., 1998. Modification of gene activity in mouse embryos in utero by a tamoxifen- inducible form of Cre recombinase. Curr. Biol. 8, 1323–1326.

De Calisto, J., Araya, C., Marchant, L., Riaz, C.F., Mayor, R., 2005. Essential role of non-canonical Wnt signalling in neural crest migration. Development 132, 2587–2597.

De Langhe, S.P., Carraro, G., Tefft, D., Li, C., Xu, X., Chai, Y., Minoo, P., Hajihosseini, M.K., Drouin, J., Kaartinen, V., Bellusci, S., 2008. Formation and differentiation of multiple mesenchymal lineages during lung development is regulated by beta-catenin signaling. PLoS One 3, e1516.

Fuchs, S., Herzog, D., Sumara, G., Buchmann-Moller, S., Civenni, G., Wu, X., Chrostek-Grashoff, A., Suter, U., Ricci, R., Relvas, J.B., Brakebusch, C., Sommer, L., 2009. Stage-specific control of neural crest stem cell proliferation by the small rho GTPases Cdc42 and Rac1. Cell Stem Cell 4, 236–247.

Fukata, M., Kaibuchi, K., 2001. Rho-family GTPases in cadherin-mediated cell–cell adhesion. Nat. Rev. Mol. Cell. Biol. 2, 887–897.

Fukata, M., Nakagawa, M., Kaibuchi, K., 2003. Roles of Rho-family GTPases in cell polarisation and directional migration. Curr. Opin. Cell Biol. 15, 590–597.

Giancotti, F.G., Ruoslahti, E., 1999. Integrin signaling. Science 285, 1028–1032.

Gilbert, S.F. (Ed.), 2006. Developmental Biology, 8th ed. Sinauer associates, Inc, Sunderland.

Glogauer, M., Marchal, C.C., Zhu, F., Worku, A., Clausen, B.E., Foerster, I., Marks, P., Downey, G.P., Dinauer, M., Kwiatkowski, D.J., 2003. Rac1 deletion in mouse neutrophils has selective effects on neutrophil functions. J. Immunol. 170, 5652–5657.

Grande-Garcia, A., Echarri, A., Del Pozo, M.A., 2005. Integrin regulation of membrane domain trafficking and Rac targeting. Biochem. Soc. Trans. 33, 609–613.

Guo, F., Debidda, M., Yang, L., Williams, D.A., Zheng, Y., 2006. Genetic deletion of Rac1 GTPase reveals its critical role in actin stress fiber formation and focal adhesion complex assembly. J. Biol. Chem. 281, 18652–18659.

Haataja, L., Groffen, J., Heisterkamp, N., 1997. Characterization of RAC3, a novel member of the Rho family. J. Biol. Chem. 272, 20384–20388.

Harlow, E., Lane, D., 1988. Antibodies. A Laboratory Manual. CSH Press, New York.

Hobert, O., Moerman, D.G., Clark, K.A., Beckerle, M.C., Ruvkun, G., 1999. A conserved LIM protein that affects muscular adherens junction integrity and mechanosensory function in Caenorhabditis elegans. J. Cell Biol. 144, 45–57.

Hogan, B., Beddington, R., Costantini, F., Lacy, E., 1994. Manipulating the mouse embryo. A laboratory manual. Cold Spring Harbor Laboratory Press, New York.

Hutson, M.R., Kirby, M.L., 2003. Neural crest and cardiovascular development: a 20-year perspective. Birth Defects Res. C Embryo Today 69, 2–13.

Ishii, M., Han, J., Yen, H.Y., Sucov, H.M., Chai, Y., Maxson Jr., R.E., 2005. Combined deficiencies of Msx1 and Msx2 cause impaired patterning and survival of the cranial neural crest. Development 132, 4937–4950.

Jiang, X., Rowitch, D.H., Soriano, P., McMahon, A.P., Sucov, H.M., 2000. Fate of the mammalian cardiac neural crest. Development 127, 1607–1616.

Kaartinen, V., Dudas, M., Nagy, A., Sridurongrit, S., Lu, M.M., Epstein, J.A., 2004. Cardiac outflow tract defects in mice lacking ALK2 in neural crest cells. Development 131, 3481–3490.

Kaibuchi, K., Kuroda, S., Amano, M., 1999. Regulation of the cytoskeleton and cell adhesion by the Rho family GTPases in mammalian cells. Annu. Rev. Biochem. 68, 459–486.

Kalcheim, C., Le Douarin, N.M., 1986. Requirement of a neural tube signal for the differentiation of neural crest cells into dorsal root ganglia. Dev. Biol. 116, 451–466.

Ko, S.O., Chung, I.H., Xu, X., Oka, S., Zhao, H., Cho, E.S., Deng, C., Chai, Y., 2007. Smad4 is required to regulate the fate of cranial neural crest cells. Dev. Biol. 312, 435–447.

Le Douarin, N.M., Creuzet, S., Couly, G., Dupin, E., 2004. Neural crest cell plasticity and its limits. Development 131, 4637–4650.

LeDouarin, 1982. The Neural Crest. Cambridge University Press, Cambridge.

Liang, X., Sun, Y., Schneider, J., Ding, J.H., Cheng, H., Ye, M., Bhattacharya, S., Rearden, A., Evans, S., Chen, J., 2007. Pinch1 is required for normal development of cranial and cardiac neural crest-derived structures. Circ. Res. 100, 527–535.

Liu, W., Selever, J., Lu, M.F., Martin, J.F., 2003. Genetic dissection of pitx2 in craniofacial development uncovers new functions in branchial arch morphogenesis, late aspects of tooth morphogenesis, and cell migration. Development 130, 6375–6385.

Liu, W., Sun, X., Braut, A., Mishina, Y., Behringer, R.R., Mina, M., Martin, J.F., 2005. Distinct functions for Bmp signaling in lip and palate fusion in mice. Development 132, 1453–1461.

Meyers, E.N., Lewandoski, M., Martin, G.R., 1998. An Fgf8 mutant allelic series generated by Cre- and Flp-mediated recombination. Nat. Genet. 18, 136–141.

Morikawa, Y., Cserjesi, P., 2008. Cardiac neural crest expression of Hand2 regulates outflow and second heart field development. Circ. Res. 103, 1422–1429.

Nakamura, H., 1982. Mesenchymal derivatives from the neural crest. Arch. Histol. Jpn. 45, 127–138.

Nichols, D.H., 1986. Formation and distribution of neural crest mesenchyme to the first pharyngeal arch region of the mouse embryo. Am. J. Anat. 176, 221–231.

Nishiya, N., Kiosses, W.B., Han, J., Ginsberg, M.H., 2005. An alpha4 integrin-paxillin-Arf-GAP complex restricts Rac activation to the leading edge of migrating cells. Nat. Cell Biol. 7, 343–352.

Pankov, R., Endo, Y., Even-Ram, S., Araki, M., Clark, K., Cukierman, E., Matsumoto, K., Yamada, K.M., 2005. A Rac switch regulates random versus directionally persistent cell migration. J. Cell Biol. 170, 793–802.

Ridley, A.J., 2006. Rho GTPases and actin dynamics in membrane protrusions and vesicle trafficking. Trends Cell Biol. 16, 522–529.

Ridley, A.J., Hall, A., 1992. The small GTP-binding protein rho regulates the assembly of focal adhesions and actin stress fibers in response to growth factors. Cell 70, 389–399.

Ridley, A.J., Paterson, H.F., Johnston, C.L., Diekmann, D., Hall, A., 1992. The small GTP-binding protein rac regulates growth factor-induced membrane ruffling. Cell 70, 401–410.

Ridley, A.J., Schwartz, M.A., Burridge, K., Firtel, R.A., Ginsberg, M.H., Borisy, G., Parsons, J.T., Horwitz, A.R., 2003. Cell migration: integrating signals from front to back. Science 302, 1704–1709.

Rose, D.M., Alon, R., Ginsberg, M.H., 2007. Integrin modulation and signaling in leukocyte adhesion and migration. Immunol. Rev. 218, 126–134.

Schmitz, A.A., Govek, E.E., Bottner, B., Van Aelst, L., 2000. Rho GTPases: signaling, migration, and invasion. Exp. Cell Res. 261, 1–12.

Soriano, P., 1999. Generalized lacZ expression with the ROSA26 Cre reporter strain. Nat. Genet. 21, 70–71.

Sugihara, K., Nakatsuji, N., Nakamura, K., Nakao, K., Hashimoto, R., Otani, H., Sakagami, H., Kondo, H., Nozawa, S., Aiba, A., Katsuki, M., 1998. Rac1 is required for the formation of three germ layers during gastrulation. Oncogene 17, 3427–3433.

Tan, W., Palmby, T.R., Gavard, J., Amornphimoltham, P., Zheng, Y., Gutkind, J.S., 2008. An essential role for Rac1 in endothelial cell function and vascular development. Faseb J. 22, 1829–1838.

Vallejo-Illarramendi, A., Zang, K., Reichardt, L.F., 2009. Focal adhesion kinase is required for neural crest cell morphogenesis during mouse cardiovascular development. J. Clin. Invest. 119, 2218–2230.

Waldo, K.L., Hutson, M.R., Stadt, H.A., Zdanowicz, M., Zdanowicz, J., Kirby, M.L., 2005a. Cardiac neural crest is necessary for normal addition of the myocardium to the arterial pole from the secondary heart field. Dev. Biol. 281, 66–77.

Waldo, K.L., Hutson, M.R., Ward, C.C., Zdanowicz, M., Stadt, H.A., Kumiski, D., Abu-Issa, R., Kirby, M.L., 2005b. Secondary heart field contributes myocardium and smooth muscle to the arterial pole of the developing heart. Dev. Biol. 281, 78–90.

Wallingford, J.B., 2005. Vertebrate gastrulation: polarity genes control the matrix. Curr. Biol. 15, R414–R416.

Wang, Z., Wang, D.Z., Hockemeyer, D., McAnally, J., Nordheim, A., Olson, E.N., 2004. Myocardin and ternary complex factors compete for SRF to control smooth muscle gene expression. Nature 428, 185–189.

Wang, J., Nagy, A., Larsson, J., Dudas, M., Sucov, H.M., Kaartinen, V., 2006. Defective ALK5 signaling in the neural crest leads to increased postmigratory neural crest cell apoptosis and severe outflow tract defects. BMC Dev. Biol. 6, 51 51.

Wu, X., Tu, X., Joeng, K.S., Hilton, M.J., Williams, D.A., Long, F., 2008. Rac1 activation controls nuclear localization of beta-catenin during canonical Wnt signaling. Cell 133, 340–353.

Yelbuz, T.M., Waldo, K.L., Kumiski, D.H., Stadt, H.A., Wolfe, R.R., Leatherbury, L., Kirby, M.L., 2002. Shortened outflow tract leads to altered cardiac looping after neural crest ablation. Circulation 106, 504–510.